Research Article

Conceptual design of a 15-TW pulsed-power accelerator for high-energy-density−physics experiments

R.B. Spielman [a],*, D.H. Froula [a], G. Brent [a], E.M. Campbell [a], D.B. Reisman [b], M.E. Savage [b], M.J. Shoup III [a], W.A. Stygar [b], M.L. Wisher [b]

[a] *Laboratory for Laser Energetics, University of Rochester, Rochester, NY, 14623, USA*
[b] *Sandia National Laboratories, Albuquerque, NM 87185, USA*

Abstract

We have developed a conceptual design of a 15-TW pulsed-power accelerator based on the linear-transformer-driver (LTD) architecture described by Stygar [W. A. Stygar et al., Phys. Rev. ST Accel. Beams 18, 110401 (2015)]. The driver will allow multiple, high-energy-density experiments per day in a university environment and, at the same time, will enable both fundamental and integrated experiments that are scalable to larger facilities. In this design, many individual energy storage units (bricks), each composed of two capacitors and one switch, directly drive the target load without additional pulse compression. Ten LTD modules in parallel drive the load. Each module consists of 16 LTD cavities connected in series, where each cavity is powered by 22 bricks connected in parallel. This design stores up to 2.75 MJ and delivers up to 15 TW in 100 ns to the constant-impedance, water-insulated radial transmission lines. The transmission lines in turn deliver a peak current as high as 12.5 MA to the physics load. To maximize its experimental value and flexibility, the accelerator is coupled to a modern, multibeam laser facility (four beams with up to 5 kJ in 10 ns and one beam with up to 2.6 kJ in 100 ps or less) that can provide auxiliary heating of the physics load. The lasers also enable advanced diagnostic techniques such as X-ray Thomson scattering and multiframe and three-dimensional radiography. The coupled accelerator-laser facility will be the first of its kind and be capable of conducting unprecedented high-energy-density−physics experiments.

1. Introduction

Since 1970, low-impedance, pulsed-power accelerators have been based on Marx-generator, water-pulse-forming technology. The world's largest and most-powerful pulsed-power accelerator is the Z accelerator [1,2], refurbished from the original facility in 2007 and located at Sandia National Laboratories (SNL) in Albuquerque, NM. Z stores 20 MJ of electrical energy at a charge voltage of 85 kV and delivers as much as 28 MA in 110 ns to a wide range of loads. Z represents the state-of-the-art for Marx-generator, water-pulse-forming accelerators, delivering greater than 2 MJ of energy to a wide range of targets. The coupling of a high-power laser beam [3] to Z has pioneered new high-energy science by providing advanced diagnostic techniques [3] and innovative fusion concepts [4].

In this article, we describe the conceptual design of a compact, highly efficient pulsed-power accelerator, based on a linear-transformer-driver (LTD) machine architecture [5,6],

coupled to a multibeam, high-power laser system. One of our key goals was to design a pulsed-power accelerator, smaller than Z, that would demonstrate and validate the LTD architecture proposed by Ref. [6] for accelerators larger than Z while coupling an advanced high-power laser system to the pulsed-power loads. Particular attention has been paid to providing extensive diagnostic access to the load while maintaining machine performance. This new LTD design would take advantage of the very efficient coupling of stored energy to the load to build a pulsed-power accelerator capable of delivering up to 12.5 MA and over 600 kJ to a range of dynamic loads for a variety of high energy-density–physics (HEDP) research.

The LTD pulsed-power facility was designed to be coupled to a laser system capable of delivering four, nominally 5-kJ ultraviolet (UV) beams with state-of-the-art beam conditioning, a pulse-shaping capability to generate 150-ps to 10-ns-long laser pulses, and a single, 2.5-kJ infrared (IR) laser beam with a pulse-width range of 1 ps–100 ps. The four UV beams will enable 3-D radiography to precisely measure the evolution of high-energy-density (HED) plasmas. Other configurations would enable auxiliary heating of a plasma and radiography in the same experiment. These laser intensities will make it possible to generate X rays with energies greater than 10 keV for novel HED physics studies, including advanced high-density radiography, X-ray Thomson scattering, and diffraction experiments.

Our conceptual design is for a pulsed-power accelerator that has a single stage of pulse compression and has a matched electrical impedance throughout, as described by Stygar et al. [6], thereby minimizing electrical reflections and maximizing overall electrical coupling efficiency to the load. Depending on the load details, coupling efficiencies as large as 25% (load kinetic energy/stored energy) can be realized. We have fixed the $\sqrt{LC}$ time constant of the prime-power store to be ~100 ns to eliminate the need for further pulse compression (with its attendant losses in efficiency). The LTD design enables longer electrical pulses by pulse shaping the current via independent triggering of the bricks. The goal is to maximize the flexibility of the driver for HEDP research.

The architecture of our accelerator is based on the generic LTD architecture described by Stygar et al. [6]. Our design assumes the use of an LTD brick based on two, 80-nF capacitors and a single, low-inductance gas switch connected
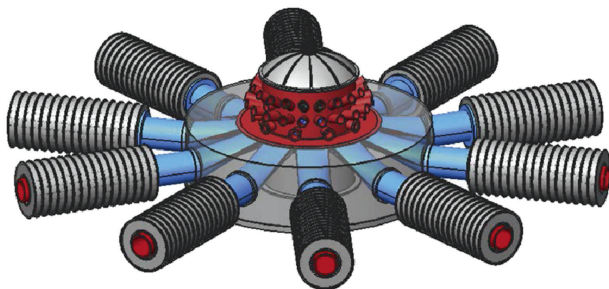
electrically in series (see Fig. 1). Multiple bricks are assembled in parallel in a cavity. The cavities are arranged in series into a single module. Multiple modules, feeding through co-axial water lines, comprise the entire accelerator and drive a single load via a tri-plate magnetically insulated transmission line.

Detailed circuit simulations using *Screamer* [7,8] model the performance of the accelerator with different loads. These simulations model all of the elements of the accelerator from the bricks (switch losses), the cavities (core losses), the modules, the water transmission lines (water losses), the magnetically insulated transmission lines (electron losses), and the post-hole convolute (vacuum-electron-flow losses) to the load. Detailed descriptions of the designs and the assumptions used in the simulations are provided in Secs. 2 and 3.

This pulsed-power accelerator could serve as the first large-scale demonstration of LTD architecture. Such a facility will facilitate a wide range of HEDP experiments that will incorporate modern pulsed-power with state-of-the-art laser capabilities. Given the research enabled by coupling the Z facility with the Z-Beamlet [3] (the successful prototype of a National Ignition Facility beamline) at Sandia, it is likely that any future pulsed-power facility of scale will incorporate multiple, high-power lasers. The facility described in this paper could therefore serve as a "prototype" for any future facility of scale [6].

2. Conceptual design for a 15-TW pulsed-power accelerator

2.1. Overview

This conceptual electrical design has performance parameters that are roughly 1/4 scale in energy and power from SNL's original Z machine (3 MV, 20 MA, 100 ns, 0.12 Ω, 60 TW) [9–12]. This new design operates at ~2 × lower peak current than the original Z and it addresses the following key design goals:

- LTD architecture and pulse shaping: The driver design is based on an LTD prime-power architecture [6]. The choice of the LTD as the prime-power source is motivated by the fundamental efficiency and pulse-shaping flexibility of LTD designs [13], the maturity of SNL's LTD engineering, the reduced maintenance of LTD components, the lack of water shock, and the technological impact to the National Pulsed-Power Program. Such a facility would also motivate and help develop the needed "supply chain" for critical components for any future, large-scale pulsed-power facility.
- The ability to efficiently drive a wide array of HEDP experiments that are scalable to present (Z) and future, high-energy pulsed-power facilities: Currents must be large enough to stably implode scaled liners to relevant velocities (~10^7 cm/s). Scalable HEDP experiments that exploit the X-ray energy and power produced by wire arrays or gas puffs are also a desired capability. The ability to

Fig. 1. Schematic of an LTD brick showing two double-ended capacitors and a single 200-kV low-inductance gas switch.

conduct dynamic materials experiments at ~1Mbar is also important.

- High shot rate, low hardware cost, manageable debris levels, and low activation: The requirement for up to two to three shots per day is driven by the desire to reduce the cost per shot (annual facility cost/shots), to increase the number of experiments conducted, and develop a user community such as what currently exists at the Omega Laser Facility. The higher shot rate encourages technically high-risk experiments that often drive innovation. To manage facility costs with high shot rates, the hardware replacement costs must be minimized and the debris level maintained below diagnostic-damage thresholds. User experience from SNL's Saturn accelerator [14] demonstrated that a peak current of ~10 MA damaged only the inner MITL hardware, had acceptable levels of debris, and had no hardware activation.

- Maximize experimental flexibility and utility, and provide equatorial diagnostic access: Flexible and multiple diagnostic ports provide optimal X-ray diagnostic and laser-beam access. The target chamber will have multiple (approximately eight) equatorial line-of-sight ports and will have further diagnostic access at ~15° and ~30° above the equator. Axial access is also planned for X-ray diagnostics, laser diagnostics, and to enable experiments that can both heat and probe the targets.

Fig. 2 shows the schematic view of the model for our 15-TW accelerator. This pulse-power design uses an LTD-based architecture having ten radial modules arranged azimuthally around the load, with each module containing 16 cavities, and with each cavity containing 22 bricks. The total electrical energy stored in all the brick capacitors within the modules is 2 MJ at a charge voltage of 85 kV (2.75 MJ at 100 kV). The modules will be placed at a single level on the main floor of the building to enable easy access for operations and maintenance; with a similar motivation, the cavities will be positioned and supported in the modules on rails. The cathode stalk in each module will be supported from the outer radial location and extend to, and be supported by, the coaxial water transmission line at the output of the module. The cathode stalk can be removed when the water is drained from the module and the
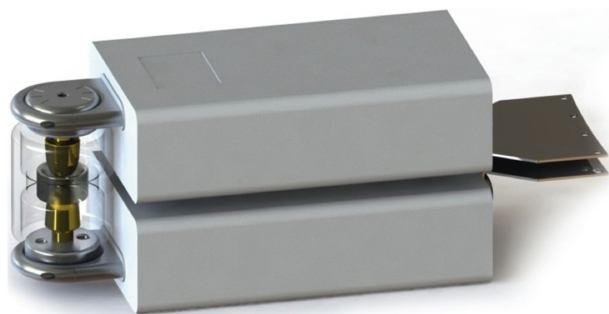

Fig. 2. Schematic of the 15-TW driver showing ten linear-transformer-driver (LTD) modules (each having 16 cavities) coupled to coaxial water lines, to the water section, and then to the inner vacuum power feed.

inner water tank (150,000 L). With the cathode stalk removed, the individual cavities can be removed from the module for maintenance or the entire module can be replaced.

Each module couples to a 2-m-long, 1.25-Ω coaxial water transmission line [15] and these coaxial, water transmission lines connect to a large water tank containing the water transmission-line convolutes. Each coaxial transmission line transitions, at constant impedance, to a horizontal, tri-plate transmission line. The ten tri-plate water lines merge into a single tri-plate, disk water line just outside the vacuum insulator stack. These water lines provide complete transit-time isolation of the cavities from the load. Each module drives a fixed 1.25-Ω load and is transit-time isolated from the load. The 0.125-Ω transmission line drives the load and the load is transit-time isolated from the modules. The transit-time isolation also serves to separate in time the reflected voltage pulse from the forward-going voltage pulse, thereby minimizing voltage stress on the cavity components.

The insulator-stack assembly consists of two, well-graded identical insulator stacks, each composed of four insulators and three grading rings. Inside the insulator stacks are two, magnetically insulated vacuum radial transmission lines (MITL's)—two anodes and one cathode—arranged in a single, tri-plate disk configuration.

Two, constant-impedance disk MITL's connect the region near the insulators with a single, post-hole convolute. The MITL's are designed with nearly the same E/cB as the SNL Z MITL's [9–12]. Inside the post-hole convolute (PHC) there is an inner disk MITL and a coaxial MITL coupling to the load. The lower voltage of this design greatly reduces the current losses seen on Z in the post-hole convolute and the inner MITL.

2.2. Brick design

The basic building block of the LTD driver is a "brick" composed of two capacitors in series and a gas-filled, spark-gap switch (see Fig. 1). The baseline accelerator design consists of 3520 bricks (3520 switches and 7040 capacitors). The two capacitors and one switch are arranged in a low-inductance, compact configuration. The key brick performance parameters are the peak current per brick (fundamentally limited by the capacitor current limit) and the rise time of the brick (set by the brick capacitance, total brick inductance, and load impedance). The larger the current per brick, the fewer bricks needed per cavity to achieve the desired cavity current. The individual brick performance effectively defines the overall electrical performance of the driver as a whole through the brick's capacitance, inductance, resistance, peak current, allowed voltage reversal, lifetime, reliability, pre-fire rate, hang-fire rate, size, and jitter. These brick parameters must be refined and quantified before the final machine design is set. Design and optimization efforts will focus on producing the lowest-possible brick inductance and highest-possible, peak capacitor current within the desired 100-ns rise time. The brick current, upon which our design is based, is presently limited by the 50-kA current limit of the individual capacitors.

Our brick design is the baseline Z300 SNL design [16−18]. Our design uses two, 80-nF capacitors arranged in a one-stage Marx configuration (two capacitors and one switch), with the switch placed between the two capacitors and the midplane of the switch at ground potential. The two capacitors can each be charged to a maximum voltage of 100 kV (SNL has demonstrated routine operation of such bricks at ±100 kV). The capacitors are the low-inductance, "double-ended" style with the electrical connections placed on opposing ends of the capacitors. The present switch is a low-inductance, high-pressure, 200-kV spark-gap design [18]. The anode/cathode gap of the gas switch is ~0.95 cm and the switch is operated at 16.5 bars of dry air. The switch is triggered by applying a fast-rising, ~50-kV pulse to the midplane of the switch (typically applied by a 50-Ω cable with a 1-kΩ resistor in series), thereby initiating an overvoltage situation with one of the electrodes. A 50-kV trigger pulse achieves a 60-ns run time and a 2.5-ns 1σ jitter. The trigger pulse must be applied to the midplane of the switch for a time corresponding to the streamer transit time from the electrode to the midplane of the switch.

Each brick has a matched impedance Z_b, where $Z_b = (L/C)^{1/2}$ (L is the total inductance of the brick and C is the total capacitance of the brick). The matched impedance is nearly optimum for power coupling to the load (Actually, the optimum load for power coupling is 1.1 Z_b but the difference from Z_b is less than 0.5% [6].) A resistance that is 2 × greater than the matched value would then be critically damped and would have no undershoot/reversal. Resistance values much lower than the matched value would have excessive voltage reversal and could damage the capacitors. A matched value for the load impedance optimizes coupling efficiency while minimizing voltage reversal.

Total resistive energy losses in the brick (~23.9%) are caused by the time-dependent resistance in the gas switch (a function of switch gap, the gas type, multichanneling, and the gas pressure) and the effective series resistance (ESR) of the two capacitors.

2.3. Cavity design

An LTD "cavity" is composed of multiple bricks arranged radially in parallel. A cavity has the same peak output voltage as a single brick, but has the total current of N_b bricks and an output impedance of Z_b/N_b Each cavity includes the necessary cathode coupling and intracavity-isolation magnetic cores to enable the cavities to be stacked in series (see Fig. 3). Bricks are arranged radially around the inner coaxial section. Common charging connections and a common pulsed-triggering system are used for all of the bricks.

During our design of the cavity, we varied the number of bricks in the cavity and, later, the number of cavities in a module to get the desired 1.25-Ω module impedance, cavity current, and output voltage. Future changes to the detailed parameters of an individual brick, which result in a changed brick matched impedance, would necessitate a change in the number of bricks per cavity and, perhaps, the number cavities per module.
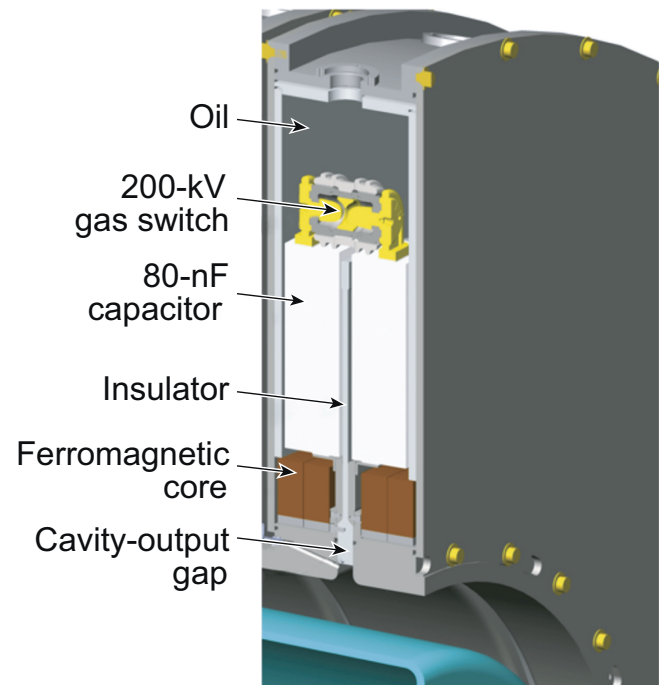

Fig. 3. Schematic of an LTD cavity showing one (of 22) bricks driving the output. The cavity contains ferromagnetic core material used to eliminate parasitic current losses. The cavity is oil filled.

The gas switches for each brick within the cavities will be triggered electrically. At *least* two, separate and independent triggering systems per cavity would be required to provide minimal pulse shaping. Multiple, independent trigger systems are needed to achieve the precise pulse shaping needed for equation-of-state experiments [13]. A typical trigger pulse will have an amplitude of ~50 kV with a rise time of ~5 ns. In test cavities, a single trigger pulse is capable of triggering ~20 switches.

Each cavity contains several ferromagnetic magnetic cores that are placed to prevent parasitic current losses (see Fig. 3). The ferromagnetic cores must have sufficient cross-sectional area to support the $V \bullet t$ of the pulse. Acceptable ferromagnetic core materials are 2605CO MetGlas™ and FT-3M™ FineMet. In addition to the fundamental requirement of supporting the pulse without saturation, core losses and winding voltage must be considered in the design. Both types of cores have been successfully tested [19].

2.4. Module design

Fig. 4 shows the conceptual design of the LTD module that feeds a 1.25-Ω impedance coaxial water transmission line. The number of cavities per module was adjusted ($N_c = 16$ cavities in series) to achieve the desired final output voltage (~1.25 MV) and the desired impedance (1.25 Ω) needed for the module. The final module output current is ~1 MA. The power generated by a single module is 1 TW at 85-kV charge voltage and a maximum of 1.5 TW at full 100-kV charge voltage.
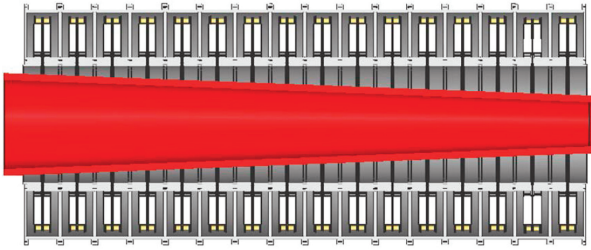
Fig. 4. Schematic of an LTD module showing 16 cavities bricks arranged in series. The module has a tapered cathode that matches the impedance of the cavities as they are added axially. The module is filled with de-ionized water.

Each module has a tapered cathode stalk as the center conductor. The diameter of the cathode stalk varies with each cavity to maintain the correct water-transmission-line impedance. After 16 cavities, the impedance of the water line is a constant 1.25 Ω.

A 16-cavity module will require a sophisticated triggering system to provide the necessary timing flexibility for the 352 switches. In fact, in many ways the triggering system for a module is a more-complicated engineering task than the module itself. Each module will have its own separate and independent trigger system. This triggering system will consist of multiple trigger units for each cavity. The cabling for the trigger systems must take into account the need to fire the cavities sequentially so as to take into account the electromagnetic propagation time of the voltage pulse in water.

As mentioned above, to maximize operability the individual cavities are mounted on the module rails so that they can be individually removed as needed for repair or refurbishment. This requires that the water be drained and the central cathode stalk be withdrawn. Once the high-voltage charging lines, trigger cables, and gas lines are removed the ~1-t weight cavity can be removed using an overhead crane. A replacement cavity would immediately be immediately installed and the module reassembled.

2.5. Water transmission line design

The water transmission lines are simple, constant-impedance coaxial designs that are manufactured from rugged stainless steel. These coaxial water transmission lines connect the output of an LTD module to the water convolutes. All of the coaxial transmission lines will meet at a water-filled tank. Inside the stainless-steel water tank, the coaxial transmission lines transition or convolute from a coaxial shape to tri-plate lines that then merge into a disk water-transmission line and then into a large, monolithic, vacuum-insulator stack.

De-ionized water will be used as the dielectric in the water transmission lines between the modules and the insulator stack. Water was chosen because of its high dielectric constant ($\varepsilon \sim 81$) and its ability to handle pulsed high voltages. The ten modules with their associated coaxial water transmission lines are arranged radially around a water tank (containing de-ionized water).

The minimum radial spacing between the outer and inner conductors of the coaxial water lines is determined by the high-voltage breakdown limit in water. In our conceptual design, we have chosen the outer diameter (OD) of the water coax to be 60 cm and the inner diameter (ID) to be 49.74 cm for a 1.25-Ω transmission line. This leads to a water gap d of ~5.1 cm. Stygar et al. [20] wrote the definitive paper on water breakdown for fast voltage pulses. The breakdown requirement for large-area water lines ($A > 10^4$ cm^2) is given by

$$E_p \tau_{eff}^{0.33} \leq 0.108, \tag{1}$$

where E_p is the peak value of the average electric field in MV/cm (V_p/d, where V_p is the peak voltage) and τ_{eff} is the effective pulse width of the voltage pulse in μs at 63% of peak voltage. As will be discussed in Sec. 3, for our case, the mean peak electric field E_p is ~0.245 MV/cm and τ_{eff} is ~0.089 μs, which yields a breakdown value of 0.110. This calculated breakdown value is just below the Stygar limit for water breakdown. This calculated breakdown value very close to the observed safe operating point on Z of 0.113 [20].

The pulsed-power design uses a single, large water tank that makes it possible to connect the LTD modules/coaxial water lines to the insulator stack. This design requires the tank to be fabricated from stainless steel and that the water in the tank be continuously de-ionized and degassed. A lid composed of multiple, wedge-shaped sections will cover the water tank to keep out debris, to minimize experimental-bay humidity, and to contain the electromagnetic-pulse (EMP) generated during a shot. The volume (150,000 L) of the water tank is minimized to limit the volume of external water storage. The inner diameter of the water section was set by the insulator stack diameter and the outer diameter of the water section was set by the need for ten modules to convolute themselves from coaxial to tri-plate. A minimum radial distance of 2 m was chosen as the minimum reasonable distance for a 60-cm-OD coaxial water line to transform into a tri-plate strip line. This distance is comparable to the convolute on Z.

The coaxial transmission line transforms into a tri-plate transmission line with constant water-line impedance (see Fig. 5). The coaxial lines deform as the inner conductor assumes a race-track oval cross section; the outer electrode splits on the sides. This convolution continues with the center becoming more planar and the top and bottom sections
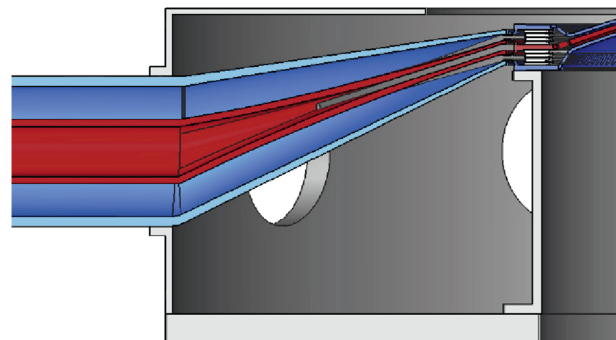

Fig. 5. Close-up of the constant-impedance transition from the coaxial water line to a horizontal tri-plate. The module is filled with de-ionized water.

assuming a planar shape. The center, top, and bottom sections become one sector of a tri-plate disk and the sectors from the ten modules merge into the disk of the insulator stack. The impedance of the water lines is constant at all locations. To meet the generic, Z water-breakdown requirement, a 0.25-Ω disk feed in the water outside of the 1.4-m-radius insulator stack will have a gap of 5.25 cm. This *A/K* gap is consistent with the water breakdown discussion above.

Modeled after the original Z insulator stack at SNL [9,10], the outer diameter of the insulator stack will be ~3 m. The overall stack diameter and disk-conductor spacing in the water was determined by the need for a 0.125-Ω impedance and limited by water breakdown in the disk section of the water transmission line just outside the insulator stack. Each level of the insulator stack will have a disk water-line impedance of 0.25 Ω. This impedance and the radius of the insulator stack set the *A/K* gap in the disk water line.

Note: the 0.125-Ω impedance driving the load is constant for the entire pulse length. This means that one can accurately model the load performance by assuming a simple, 0.125-Ω driver with the calculated voltage pulse at that location rather than the complex multicomponent model used in the calculations described below.

2.6. Insulator-stack design

The insulator-stack assembly consists of two identical insulator stacks, each composed of four Rexolite™ insulators that are ~2.5-cm high. Three hard-anodized aluminum grading rings separate the insulators and extend from the water section into the vacuum section. The insulators are capacitively graded and must be designed to have a uniform grading to within a few percent of the electric field.

Fig. 6 shows the insulator stack that separates the water section of the pulsed-power machine from the vacuum section. Its design must not only take into account the pulsed-power engineering limits, but also mechanical engineering issues (structural integrity, vacuum quality, and lifetime). The insulator-stack/vacuum interface has the lowest limit on electric field in the pulsed-power chain. As such, it is the weakest link in the entire pulsed-power chain. The maximum

Fig. 6. Schematic of an insulator stack showing four −45° Rexolite™ insulators. The insulators have anode plugs similar to Z.

surface electric field permitted in the water near the vacuum insulator for a 100-ns pulse width is ~300 kV/cm. The maximum mean electric field at the insulator stack in the vacuum is ~150 kV/cm.

Given an impedance of 0.25 Ω per disk level and the minimum allowable gap in the water (set by the applied voltage pulse and the breakdown limit in water), the outer radius of the insulator stack is fixed. The height of the insulator stack is always greater than the constant-impedance water gap because the breakdown field on the plastic−vacuum interface is lower than that of water. This creates an unavoidable impedance mismatch on the water side of the insulator stack and excess inductance in the insulator volume and in the vacuum.

Improvements to the insulator design, which increase the maximum electric field at the vacuum interface, yield a significant improvement in machine performance by decreasing the impedance mismatch in the water, reducing the inductance in the insulator stack, and lowering the inductance of the local vacuum section. SNL's Z Machine was originally designed to operate at a mean electric field of 90 kV/cm in vacuum using Rexolite™ insulators. Experiments on Z demonstrated successful, routine insulator operation at 125 kV/cm. When Z was rebuilt, further improvements were made in the insulator stack design to increase the insulator design point to 150 kV/cm [21,22]. The insulator planned for our design is nearly identical to the Z insulator stack with the exception that the area of each insulator stack is ~0.30 as large as each Z insulator (A and B levels of Z). This means that our insulator should be able to achieve a slightly higher field stress than Z based on the statistical area effects described by Stygar [21,22]. Equation (2) shows the scaling relationship for a single 45° Rexolite™ insulator:

$$E_{\mathrm{p}}\left(t_{\mathrm{eff}}C\right)^{1/10}\exp(-0.24/d) = 248, \qquad (2)$$

where E_{p} is the peak electric field across the insulator, C is the circumference of the insulator surface, and d is the height of the insulator. The effective pulse width t_{eff} is defined as

$$t_{\mathrm{eff}} \equiv \frac{1}{E_{\mathrm{p}}^{10}} \int_0^t E^{10}\mathrm{d}\tau. \qquad (3)$$

Further experiments at Sandia on Sphinx [23] demonstrated successful operation of a multi-ring insulator stack at mean electric field greater than 210 kV/cm (although for shorter pulses). The implication of the Z data and the Sphinx data is that our design for a well-graded Rexolite™ insulator stack is conservative and should be capable of handling more than 150 kV/cm.

In our design, the insulator stack must hold off a peak voltage of 1.5 MV at the vacuum/insulator interface. Based on the discussion above, the insulator design point is a conservative, peak-mean electric field of 150 kV/cm. This gives an insulator design height of ~10 cm. Fig. 7 shows the preliminary insulator design that uses four 2.54-cm-high insulators (10.16-cm total plastic height) and three 6.4-mm-thick
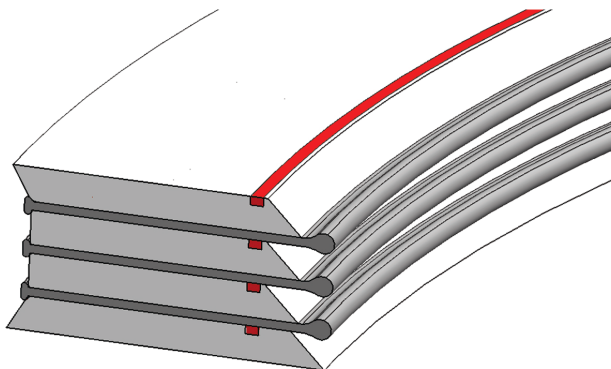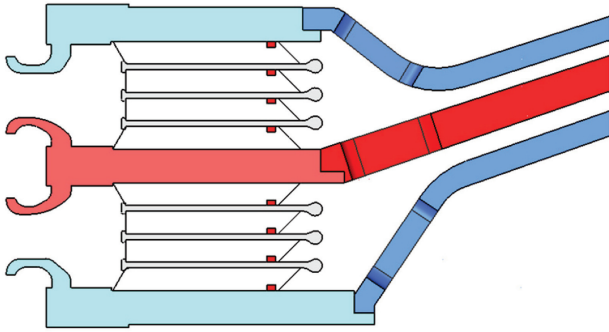
Fig. 7. The tri-plate magnetically insulated transmission line (MITL) assembly is mounted to the insulator stack. The grading rings are progressively further from the anode to maintain a local electric field below 300 kV/cm.

grading rings. The total height of the insulator stack is 12 cm. The grading rings are spaced sufficiently far from the anode disk feed to keep the local electric fields below the emission threshold of 300 kV/cm for hard-anodized aluminum. Emission from the grading rings would distort the grading of the insulator stack and likely cause the stack to flash over in the vacuum. Our design addresses this concern.

2.7. Magnetically insulated transmission lines

Fig. 8 shows the overall vacuum feed design that uses a simple, tri-plate MITL arrangement. The MITL mechanical design is based directly on the Z MITL's [1,2,9–12]. The key differences are.

- the minimum gap between the anode and the cathode will be ~1/2 the gap on Z (while E/cB will remain the same as Z),
- the 18.6° angle of the MITL's will be slightly larger to ensure that the load is accessible to diagnostics on the equatorial plane, and
- the resulting vacuum electron flow in the MITL's will be slightly lower.

This is the largest accelerator that can efficiently use two insulator-stack/MITL levels. Our design essentially uses only the top two MITL's of the four-level Z design. The A and B levels of Z had five, 5-cm-high insulators to hold off 3.0 MV. This height added inductance to the "vacuum-flare" and impedance to the "water-flare" regions. This new insulator stack design will have four, 2.5-cm-high insulators. This will reduce the inductance of the water flare, the insulator stack, and the vacuum flare to half that seen on Z, resulting in an increase in coupling efficiency to the load (see Fig. 9).

Fig. 9 shows the anodes plunging rapidly toward the cathode disk just inside the insulator stack to minimize the vacuum-flare inductance. The large diameter of the insulator stack reduces the inductance of the vacuum flare volume. The radial spacing between the anodes and the adjacent insulator grading rings is limited by the need to keep the electric field on the grading rings below 300 kV/cm at all times to prevent electron emission of the grading rings. As the anode disk
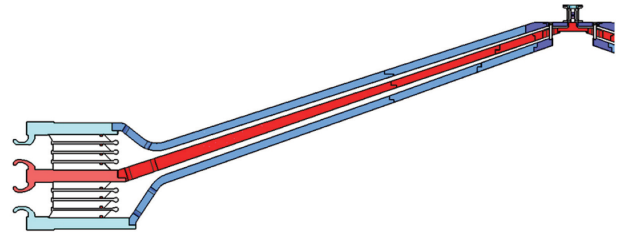

Fig. 8. Schematic of the proposed MITL's showing the transition from the insulator stack, the constant-impedance MITL, the post-hole convolute, and the load.

approaches the cathode disk, the electric field on the cathode exceeds the self-emission threshold of ~250 kV/cm and the electrodes emit electrons and the transmission line acts as an MITL. Magnetic insulation is established by a carefully tailored transition from the non-emissive cathode near the insulator to the emissive inner cathode. The cathode will be made from 304L stainless steel. The anodes will be fabricated either from aluminum or stainless steel at large diameters and stainless steel at diameters <1.5 m.

After the vacuum-flare region, the MITL's will have almost constant impedance. This is an attempt to create a vacuum feed with nearly constant E/cB similar to Z. Fig. 10 shows constant impedance MITL's that extend from the vacuum flare to the post-hole convolute. This means that the gap in the MITL's decreases from an initial value of ~10 cm to a final gap of ~0.5 cm. The MITL's are designed with nearly the same initial E/cB as the SNL Z MITL's. Our design has a similar (or lower) vacuum electron flow in the MITL's to SNL's Z. The constant impedance in the MITL means that the amount of electron current and the spatial extent of the electron sheath flowing in the vacuum will be constant over the entire radial length of the MITL. Of course, the consequence of constant impedance is that the gap of the MITL decreases inversely with the radius. This design limits the final A/K gap at the inner radius of the disk MITL from ~0.5 cm to 1.0 cm. Z uses
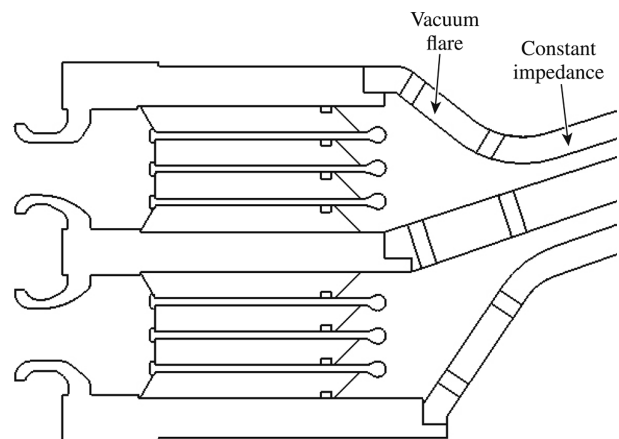

Fig. 9. Close-up of the MITL's near the insulator. Specifically, the vacuum-flare region of the vacuum feed shows the transition between the insulator stack and the constant gap of the MITL.
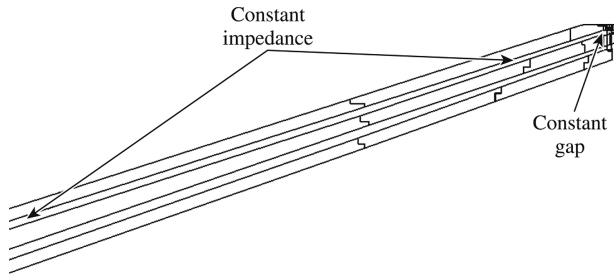
Fig. 10. Close-up of the MITL's between the vacuum flare and the post-hole convolute. Here the MITL's have a constant impedance until the post-hole convolute where the feed is a constant gap.

constant 1.0-cm *A/K* gaps in the region near the post-hole convolute.

The two MITL levels of the accelerator will be coupled to the load via a single post-hole convolute (Fig. 11) [9,10,24]. In this design, 12 anode posts penetrate 12 cathode holes to couple the upper and lower anodes. Like all current-adder convolutes, this design generates 12 magnetic-field nulls in the upper disk and 12 magnetic-field nulls on the lower disk. This is exactly the same as the magnetic-field nulls on Z. The current flow in the cathode flows on the metal surface from the lower side of the cathode plate to the upper side of the plate through the holes in the cathode. At the post-hole convolute, a constant gap is used (increasing impedance radially inward). All vacuum electron flow is assumed lost to the magnetic-field nulls in the convolute. This is a worst-case assumption but it was found to work very well on Z [9−12,24]. The lower voltages found in this MITL design will decrease the total and fractional current loss at the convolute compared with Z. The anticipated lifetime of the lower anode will be > 25 shots; the lifetime of the cathode (PHC) and the anode insert will be one shot.

There is a short disk MITL and a coaxial MITL inside the PHC (see Figs. 11 and 12). This portion of the MITL leading to the load can have many shapes depending on the specific details of the actual load. Typically, these MITL's are constant gap designs and operate with the smallest gap possible. There are many goals for the inner MITL design: low inductance, low electrical losses, low debris generation, and low X-ray flux into the MITL's.
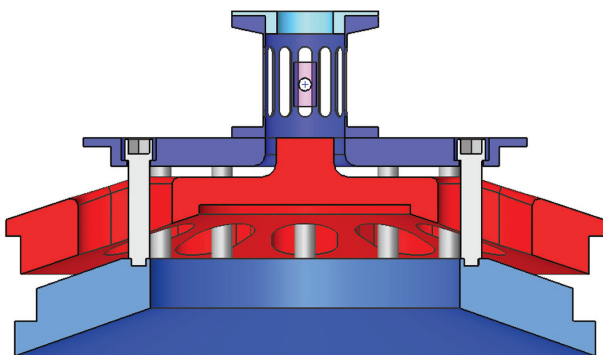

Fig. 11. The tri-plate MITL's are coupled by a post-hole convolute. The convolute is similar to a single level of the Z convolute.
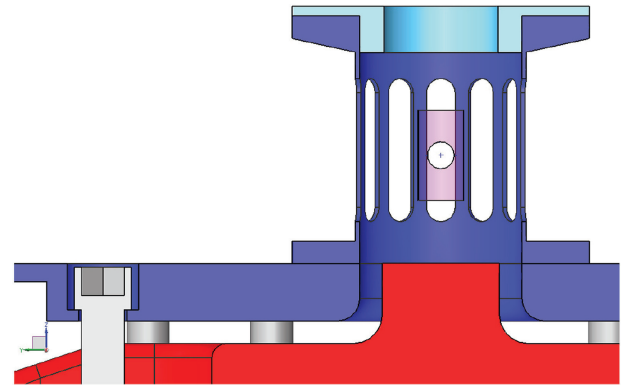

Fig. 12. Close-up of the inner coax MITL's. The MITL's have a constant gap and can be illuminated with radiation from the load.

The inner-most part of the MITL, shown in Fig. 12, sees the harshest electrical and radiation environment. The physics associated with current losses in the inner MITL [where high magnetic fields ($B > 100$ T); high, linear current densities ($J \sim 200$ MA/m); and high voltages ($E > 1.5$ GV/m) are present] is poorly understood and could potentially be one of our major programmatic R&D efforts. We anticipate minimal losses in our MITL design but such current losses could seriously impact the performance of proposed drivers having currents greater than 40 MA.

The inductance per unit volume in the MITL volume increases tremendously as the radius decreases, making inner-MITL mechanical design critical. It is essential that the inductance of the inner MITL be as low as possible. This drives the MITL design to small *A/K* gaps. A conservative gap of 5 mm was routinely used on Z and 4-mm gaps were tested [10−12].

One of the critical aspects of the inner-MITL load hardware (radius < 15 cm) is cleanliness to minimize surface plasma formation. All hardware will be built from 304L (low-carbon, low-sulfur) stainless steel. To minimize surface plasmas, the hardware must be electropolished, vacuum baked, hydrogen fired, and electroplated with gold. The hardware is handled with rubber gloves and is stored in dry air boxes. Vacuum procedures would be developed to minimize surface contamination and novel fiber-laser cleaning techniques that have been developed for other industrial applications would also be worthwhile to explore.

2.8. Diagnostic access

To maximize the physics value obtained for each shot, it is critical to have excellent diagnostic access to the load. The original Z MITL's made it possible to access to the load at ~15° off the equator of the load. This conceptual design provides perfect equatorial access to the load to provide improved diagnostic and laser-beam access. To achieve equatorial access, the MITL's must be angled by 18.6° to bring the position of the load up 10 cm to a level above the top of the upper insulator support ring. This is helped by the low height of the insulator stack. Even with no change in the MITL angle from

the Z MITL angle, the load position would have resulted in a minimum diagnostic angle of ~5°. Fig. 13 shows a top view of the equatorial access to the load.

The overall facility was designed with particular attention to diagnostic access. Diagnostic equipment load locks (DELL's) on the equator provide ~15-cm-diam diagnostic access ports to the target chamber after the load has been assembled and the target chamber has been pumped down to vacuum. The DELL's will consist of two flexible sections to provide rapid diagnostic reconfiguration and alignment. They are capable of delivering front-end diagnostic parts (e.g., pinholes, X-ray crystals, optics, fiber optics, shielding) into the target chamber. This load box will be accessed outside of the target chamber to avoid interference with the Operations Team during cleaning and reconfiguration of the main pulsed-power load. Behind the load box, a universal coupling will connect the load box to the active diagnostic package (see Fig. 13). The active diagnostics package will be a flexible box with common external mounting points to the system. Each active diagnostic package will be preconfigured off-line and rigged into the DELL as a unit. The figure also schematically shows the placement of four laser beams, including the option of injecting one beam along the axis of a cylinder.

3. Circuit modeling

Our electrical performance goals are: a peak power of 15 TW (100-kV charge), a peak current to a standard Z-pinch load of ~10 MA (85-kV charge), a total forward-going energy of ~1.7 MJ, and a current rise time of ~100 ns. These electrical performance levels should enable radiated X-ray energies of ~750 kJ and X-ray powers of ~60 TW from a tungsten wire-array load [25].

This section describes the detailed circuit modeling of a baseline LTD brick, an LTD module, a short circuit, a wire-array Z pinch, and a magnetized liner inertial fusion (MagLIF) target to illustrate the flexibility of our design. All of the circuit modeling is conducted with the latest version of

Screamer [7,8]. Appendix A contains a sample *Screamer* run deck used in Sec. 3.4.

3.1. Modeling the performance of an LTD brick

We have conducted extensive circuit modeling of the baseline LTD brick planned for our accelerator. This brick, as described above, has two 80-nF capacitors and a gas switch in series. The model includes a fixed load resistance, which together with the capacitor effective-series resistance (ESR) and the time-dependent, gas-switch resistance, approximates a matched load impedance. The total energy stored in the brick at a 100-kV charge voltage is 800 J.

We fit the circuit calculations to brick electrical measurements provided by Wisher [26] to validate the *Screamer* model. In this case, we model the switch resistance using the variable switch model in *Screamer* developed by T. H. Martin [27]. This switch model is based on a Braginskii pinch that assumes a nearly constant plasma resistivity (dielectric dependent) and a varying-arc channel diameter to meet the pressure equilibrium requirements.

Fig. 14 shows the brick current calculated by *Screamer* compared to SNL data. The simulation assumes a total brick inductance of 121.5 nH, an ESR of 0.14 Ω, and a load resistance of 2.1 Ω. The Braginskii–Martin model assumes the use of an air dielectric at 16.5 bar, a switch gap of 0.95 cm, and a single-arc channel. The initial switch resistance was chosen to be 10 GΩ. The calculation runs with a 2-ps time step to help model the changing resistance of the switch. The only real adjustment to the model was the total inductance of the circuit (poorly known). The brick delivered a peak current of 48 kA in 100 ns at a charge voltage of ±100 kV. The circuit delivered a total of ~10 mC to the load. The gas switch dissipates ~111 J (13.9%) and the capacitor ESR dissipates ~72.6 J (9%). These calculations demonstrate the importance of designing capacitors and switches with lower resistive losses.

An analysis of the calculation shows that the *Screamer* circuit model matches the data nearly perfectly for a full cycle of the current. The simulation only deviates in the start of the second cycle. Note, these data were taken using a liquid (salt)
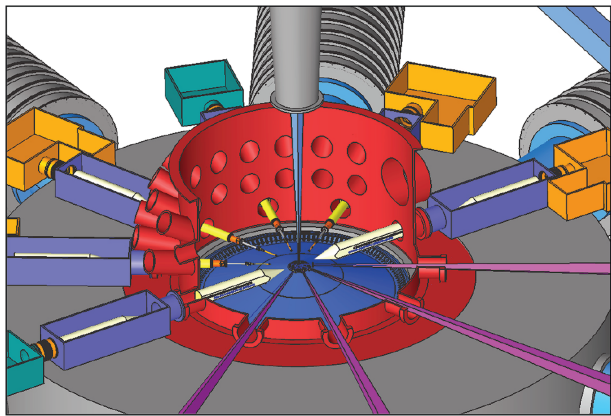

Fig. 13. Schematic of X-ray diagnostic access and laser access on the equatorial plane to the load. Several diagnostic equipment load locks (DELL's) are positioned around the chamber. The active diagnostics package can be adapted to meet the experimental needs.
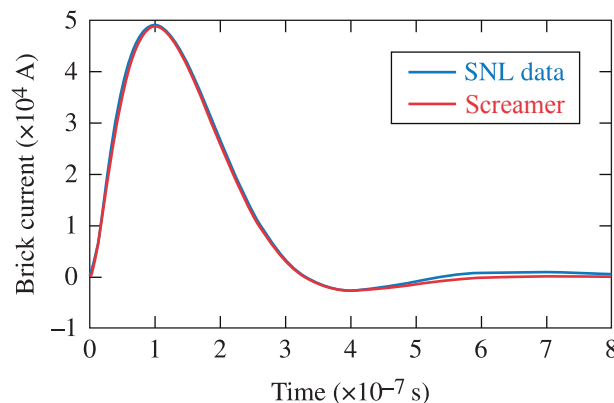

Fig. 14. The current calculated by *Screamer* (red line) compared to the measured current (blue line).

load resistor, whose resistance may vary as energy is deposited into the liquid.

It is instructive to plot the calculated resistance of the high-voltage gas switch as a function of time (see Fig. 15). The initial resistance of the switch is > 500 kΩ early in time. This resistance rapidly falls as the driving current increases and the arc channel expands. The resistance falls monotonically in time as the pulse progresses. Even at peak current (~100 ns) the resistance of the switch is ~0.3 Ω. This is a sizable fraction of the matched impedance for the brick. After the peak current, the arc channel continues to expand and the resistance of the arc continues to fall. The initial switch resistance used in *Screamer* for this calculation is 10 GΩ. The choice of the initial condition does not affect the resultant resistance as a function of time.

Comparison with data allows us to conclude that *Screamer* is capable of accurately modeling the resistive behavior of a high-voltage gas switch in the parameter range of interest. We have demonstrated predictive capability in the design of improved gas switches.

3.2. Modeling the performance of an LTD module

A single LTD module is composed of 16 individual cavities (arranged in series). Each cavity is composed of 22 bricks in parallel. We have built a *Screamer* model of a module that is terminated in a 1.25-Ω resistance. This made it possible to calculate the performance of this module as if it were installed into the full driver. The charge voltage for the capacitors in the bricks is ±85 kV. The ferromagnetic core losses from all of the cavities are included in the model [19,20].

Fig. 16 shows a plot of the module current delivered to the load resistor. The peak module current exceeds 1 MA. The current rises to a peak value in ~100 ns. Fig. 17 shows a plot that the peak power into the load resistor is 1.3 TW.

Fig. 18 shows the forward-going energy of the module. The peak energy from one module is 170 kJ. Fig. 19 shows the output voltage of the module. The peak module voltage is 1.25 MV.

In summary, the module delivers ~1.3 TW or 1/10 of the expected 13 TW from the entire accelerator. The current and
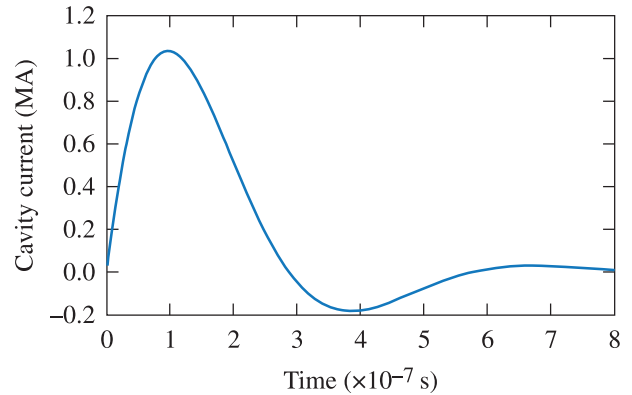

Fig. 16. Plot of the current generated by the LTD module into a 1.25-Ω load. The peak current is 1.05 MA. The rise time of the current is ~100 ns.
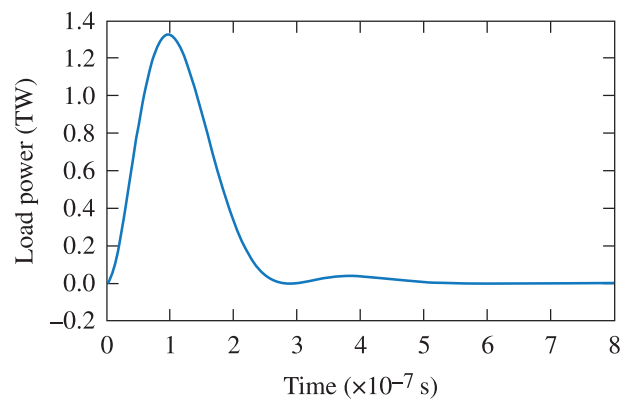

Fig. 17. Plot of the power generated by the LTD module into a 1.25-Ω load. The peak power is 1.3 TW.

voltage from the module are acceptable and will lead to the desired driver. The module is incredibly efficient in delivering energy from the capacitors in the bricks to the load. One module stores ~200 kJ of energy and delivers 170 kJ in forward-going energy. This is an efficiency of 85%. This should be compared with the typical 25% efficiency seen in Marx-driven, water-pulse–forming architectures.
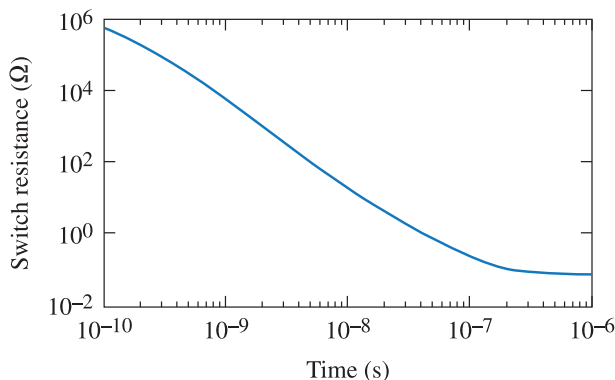

Fig. 15. Plot of the switch resistance calculated by *Screamer* as a function of time.
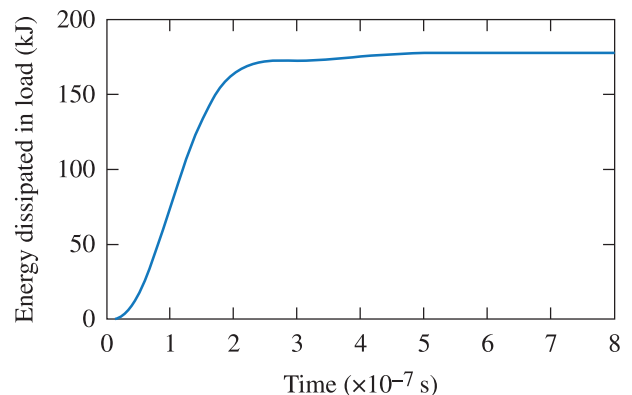

Fig. 18. Plot of the forward-going energy from the module. The total energy in the main pulse is 170 kJ.
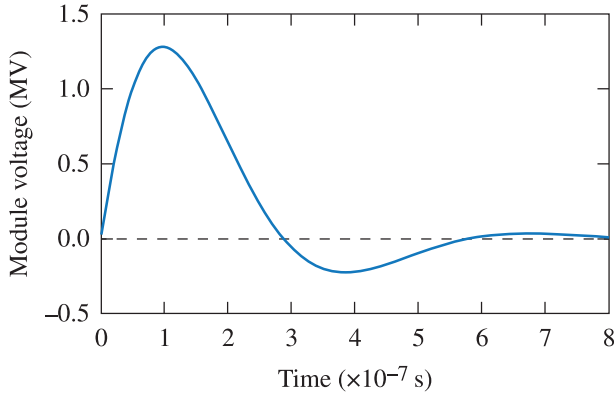
Fig. 19. Plot of the output voltage from the module. The peak voltage is 1.25 MV.

3.3. Modeling 15-TW driver short-circuit performance

It is instructive to model the performance of the 15-TW driver when the load is a short circuit. We charged the capacitors to ±85 kV for this simulation. This makes it possible to follow the movement of energy in the system without storing energy in kinetic energy. It is also a benchmark for the potential performance of the accelerator when short-circuit equation-of-state loads are used [28]. We use the same physical dimensions (inductance) for the vacuum power feed as the Z-pinch load.

The current waveforms are shown in Fig. 20. The current is determined at the insulator stack in the MITL's and the load. The vacuum electron-flow loss current is also calculated. Because of the low voltages seen on a short-circuit calculation, there are negligible electrical losses during the setup of magnetic insulation early in the pulse and there are no vacuum power-flow losses during the rest of the pulse. The peak current seen is 13 MA and the time to peak current is ~125 ns. The *Screamer* model does not presently allow the insulator to flash on voltage reversal at the insulator stack as would happen under normal operating conditions. This lack of insulator flashing does not affect the energy coupled to implosions that occur prior to voltage reversal.
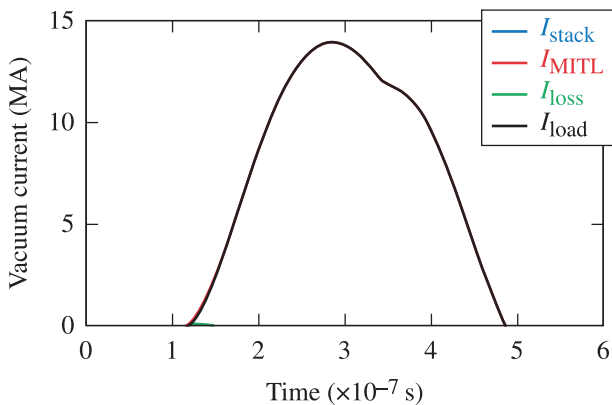
Fig. 21 plots the voltage at various locations in the vacuum transmission line. As expected, the voltage falls as the enclosed inductance is reduced ($V \sim L \, dI/dt$). For the short-circuit case, the peak voltage at the insulator stack is 1.4 MV. Voltage reversal on the insulator stack occurs at ~285 ns.

In summary, circuit simulations of our accelerator design with a short-circuit load show peak currents that are ~13 MA with no current losses seen in the MITL. The calculated voltage at the insulator stack is lower than the 1.5-MV design point for the stack, leading to added safety margin.

To illustrate the experimental possibilities of such a facility, we describe below two load examples: a wire array and a MagLIF implosion. Other loads (dynamic hohlraums, gas puffs, and loads for material studies) are also possible and will be the focus of future publications.

3.4. Wire-array Z-pinch performance

One of our pulsed-power driver design goals was to deliver ~10 MA to a tungsten wire-array Z-pinch load given a total stored electrical energy of ~2 MJ (±85-kV charge voltage). This load will result in the highest stress to the insulator stack because of the higher initial inductance of the imploding load. We modeled a standard SNL Z-pinch load having an initial radius of 2 cm and a length of 2 cm. The initial mass of the load was 1.5 mg. There was a 6-ns-long impedance mismatch (0.125-Ω to 0.250-Ω taper) in the water section outside the insulator. The total insulator and vacuum inductance was 10.82 nH.

The *Screamer* results are shown below. We calculated a peak current at the load of 10 MA, a peak load kinetic energy of 450 kJ, and a peak implosion velocity of 77 cm/μs. These calculated results are very close to scaled Z-pinch performance from Z and have a high confidence of yielding up to 750 kJ and 60 TW of X-ray radiation from a tungsten Z pinch. The Z pinch can radiate more energy than the simple 0-D model suggests because of the availability of ~500 kJ of magnetic energy around the pinch and 2-D effects in energy coupling

Fig. 20. Plot of the current at different locations in the vacuum section. The peak current is 13 MA and the loss current is negligible.
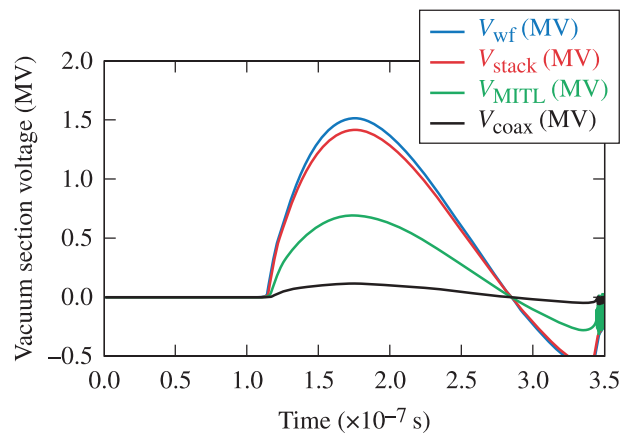

Fig. 21. Plot of the voltage at different locations in the vacuum feed. The peak voltage at the insulator stack is 1.4 MV.

[29]. The coupling from the LTD modules to the water transmission line is 83.5%. The coupling from the water transmission lines to the vacuum section by the time of implosion is 50% and the coupling efficiency to kinetic energy (KE) is ~25%. On Z the coupling efficiency from the Marx generator (13.5 MJ) to the load kinetic energy (1.1 MJ) was ~8%. We anticipate that the radiation production efficiency (X-ray energy/energy in the modules) on the LTD design will approach 35%.

Fig. 22 shows the voltage waveform at the output of the LTD module and at the beginning of the coaxial water line——still ~100 ns from the insulator stack. The key points here are: (1) the peak voltage is ~1.27 MV and is 15% less than the ideal matched voltage of 1.496 MV because of the ESR of the brick and the slight core losses and (2) the reflection in the voltage waveform from the mismatched dynamic load is delayed enough so as to minimize any overvoltage on the cavities. This is one reason that a long water transmission line is needed. The long water lines give the modules a constant load impedance and provide sufficient delay to prevent significant undershoot or overshoot on the components of the cavities.

Fig. 23 shows the current waveform at the output of the LTD module and at the beginning of the coaxial water line. The total peak current from all ten modules is 10.15 MA. The current from the reflected voltage pulse cancels the forward-going current at the time the reflection reaches that point at the exit of the module. The rise time of the current waveform is ~100 ns.

Fig. 24 shows the total forward-going energy in all ten coaxial water lines. This waveform is calculated as the integral of the total water line power in Fig. 25. The peak energy going forward in the water transmission lines is calculated to be 1.7 MJ at an 85-kV charging voltage. This is compared to the total stored energy in the modules of 2.035 MJ. The coupling efficiency from the LTD modules to the water transmission lines is 83.5%. Some of this efficiency loss is caused by resistive switch losses and the ESR of the capacitors (0.24 Ω) or ~15% of the matched, 2-Ω brick impedance.

Fig. 23. Plot of the current waveform at the beginning of the water transmission lines. In this case, the peak machine current is 10.15 MA.

Fig. 24. Plot of the energy waveform at the beginning of the water transmission lines. In this case, the peak machine energy delivered to the water transmission lines is ~1.7 MJ at a ±85-kV charge.
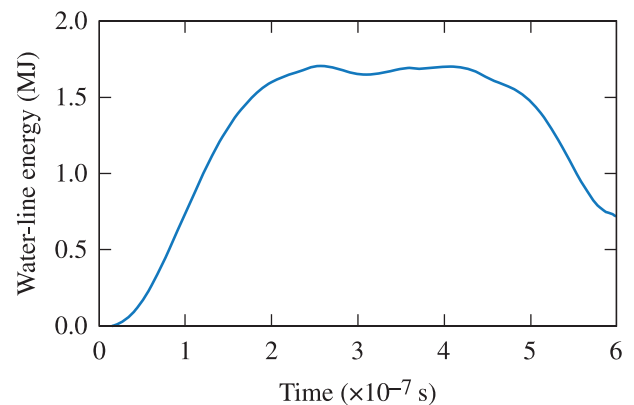
Fig. 25. Plot of the power waveform at the beginning of the water transmission lines. In this case, the peak machine power is ~13 TW at a ±85-kV charge.
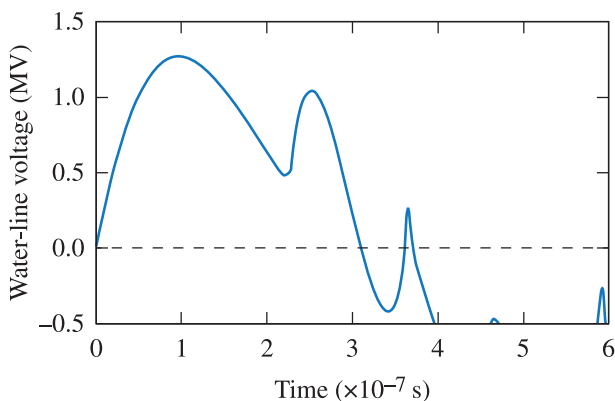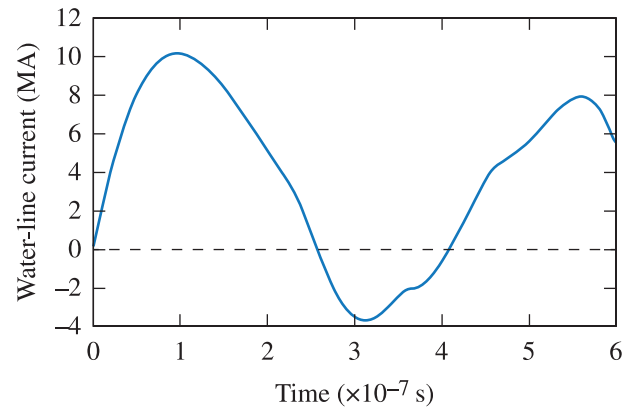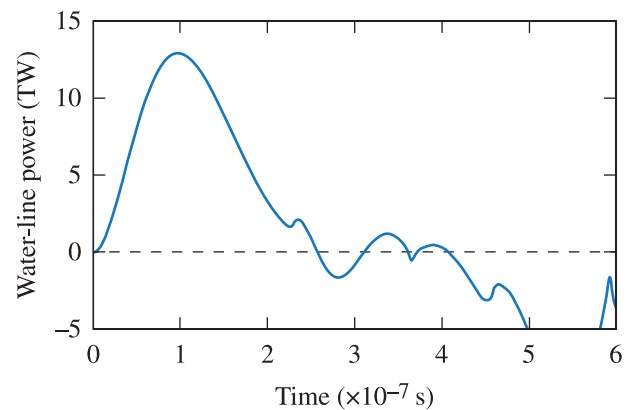

Fig. 22. Plot of the voltage waveform at the beginning of the water transmission lines. In this case, the peak voltage is 1.27 MV and a reflection from the load can be seen after 200 ns.

The various voltage waveforms are shown in Fig. 26. These waveforms are the voltage in the water outside the insulator stack before the water flare (blue curve), the voltage at the vacuum side of the insulator stack (red curve), the voltage in the MITL's prior to the convolute (green curve), and the voltage at the base of the load (black curve). There are several points of interest. First, the peak voltage on the insulator stack

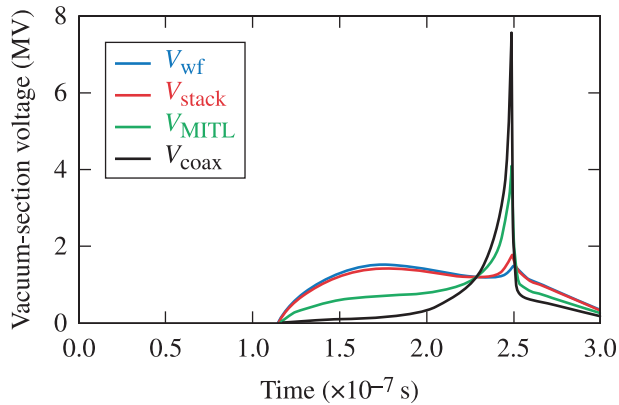Fig. 26. Plot of the voltage waveforms in the vacuum section. The peak voltage at the insulator stack is 1.42 MV and the voltage generated by the load is seen.

is 1.42 MV. Given a 10.16-cm-high insulator stack the peak, mean electric field on the insulators is 145.7 kV/cm. This is slightly under the design point discussed later in this report of 150 kV/cm. Second, the τ effective for this voltage waveform (the width of the waveform at 89% of the peak value) is 55 ns. This is the time scale that is used in various insulator breakdown calculations. Third, the impact of the target dynamic implosion inductance on the voltage at various points in the vacuum is shown. The voltage near the load achieves a 0-D value of ~7.5 MV. This "ideal" 0-D calculated voltage will be higher than the actual voltage; regardless, the voltage generated at the time of implosion will be significant and of the order of 4−5 MV. The voltage is strongly dependent on load dynamics and peak driver current. The original Z was observed to generate load voltages well in excess of 8 MV (the activation threshold for protons on steel hardware), which resulted in radioactive load hardware. Given the peak voltage in this design, we should avoid activation.

Fig. 27 shows the current delivered to the vacuum insulator stack (blue curve), the vacuum MITL (red curve), the Z-pinch load (black curve), and the loss current (green curve). Note, the loss current in the calculation reaches only ~50 kA at peak

current and reaches 830 kA at the moment of stagnation. There is a slight amount of loss during the setup of magnetic insulation at the beginning of the current pulse. The total loss at peak current is ~0.5% and is energetically insignificant. The total loss at peak current on Z for an equivalent load is ~8%, which is a significant loss in energy delivered to the load.

Fig. 28 shows the energy balance past the insulator stack (blue curve), at the MITL (red curve), and kinetic energy at the load (green curve). The energy coupled to the total inductance of the vacuum feed (past the insulator stack) reaches ~1.04 MJ at the time of implosion. The energy in the magnetic field near the load (red curve) reaches ~900 kJ. This is the energy that is directly available to the load on a time scale of approximately nanoseconds. The kinetic energy delivered to the imploding load reaches 450 kJ. In this design, the energy-coupling efficiency from the stored energy in the capacitors to the load is ~25%. This should be compared to a coupling efficiency to kinetic energy in a similar load of ~8% on Z.

Fig. 29 shows the power delivered to the imploding load. The power pulse is less than 10 ns FWHM. This represents the transfer of energy stored in the magnetic field into the kinetic energy of the load. In the circuit model this can be seen as the work done by the current against the change in inductance of the load ($I \, dL/dt$). This power can be thought of as the maximum radiated power from the pinch. While this is a 0-D circuit simulation, with all of its inherent physics limitations, the power predicted by *Screamer* was in remarkable agreement to the measured total X-ray power from tungsten wire arrays on Z [9,10].

In summary, our design is simulated to implode standard Z pinches of the type fielded on Z without pulsed-power difficulties. The voltage generated in the water transmission lines is consistent with established water breakdown criteria. The insulator stack is robust with the peak voltage leading to a peak, mean electric field at the insulator/vacuum interface that is lower than that used on Z. The MITL's have significantly lower electron losses than Z. The coupling of the electrical energy to the Z pinch scales to Z with a peak kinetic energy that is similar to the 10-MA Saturn accelerator. We anticipate radiated X-ray powers of ~60 TW and a total radiated X-ray
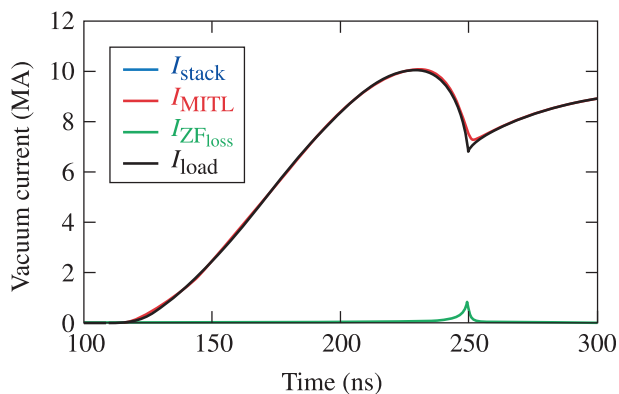

Fig. 27. Plot of the current at the insulator stack (blue), in the MITL's (red), and reaching the load (black). The loss current (green) shows that the current loss at peak current is at ~0.5% and the current loss at stagnation reaches ~12%.
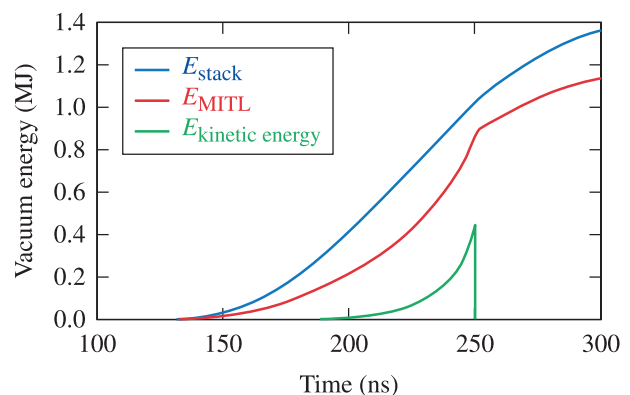

Fig. 28. Plot of the energy reaching the insulator stack (blue curve), the energy past the MITL (red curve), and the load kinetic energy (green curve).
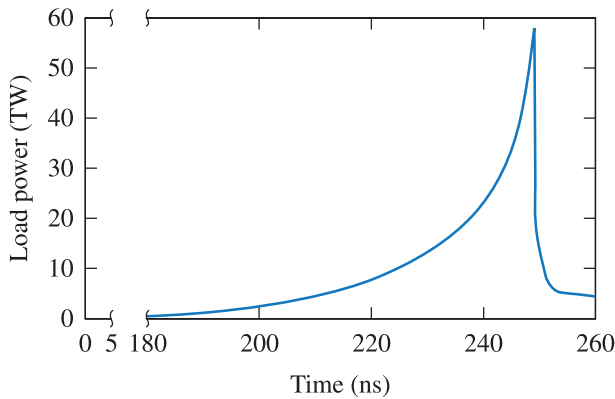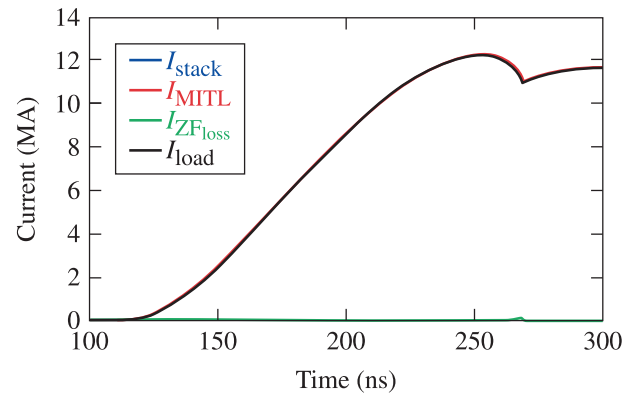
Fig. 29. Power coupled to the imploding load.

Fig. 30. Plot of the current at the insulator stack (blue), in the MITL's (red), and reaching the load (black). The loss current (green) shows that the current loss at peak current is negligible and the current loss at stagnation reaches ~1%.

yield of ~650 kJ. This is in general agreement with X-ray powers measured on the 20-MA Z Machine [25].

3.5. Magnetic liner inertial fusion target performance

Another example of a HEDP/fusion target concept that could be studied and would benefit from our 15-TW accelerator is MagLIF [4]. Such implosions could be studied while using state-of-the-art beam conditioning to understand and improve laser coupling while the other beams could be used for various diagnostic applications such as in-flight radiography. The baseline MagLIF load for our accelerator design is a Be cylinder having a total mass of 56.8 µg. The wall thickness is 243 µm. The liner outer radius is 2.79 mm and the liner length is 7.5 mm. The liner aspect ratio ($r/\Delta r$) is 11.5, similar to those used in present Z experiments. The length and the diameter of the load are identical to those of Z MagLIF targets but the mass is scaled downward from the Z values to match our peak current. We modeled the implosion of this load with our baseline 15-TW accelerator. The only changes to the inductance (compared with the Z-pinch inductance) were increases to the inner MITL feed inductance and to the inductance of the region around the load. Given the low voltage of our design, we do not anticipate significant current losses. The total insulator and vacuum inductance used in the calculation was 14.72 nH. We do not include an axial magnetic field in the design but experience at SNL and LLE gives us confidence that this presents no issue and the β (plasma pressure/magnetic-field pressure) in MagLIF is sufficiently large so as not to influence the hydrodynamics.

Fig. 30 shows the results of our simulation delivered a peak current of 12.5 MA to this MagLIF load at an 85-kV charge. Note that the minimal change in inductance of the load during the implosion allows the peak current rise much higher than the 10-MA current shown in Fig. 27 with a Z-pinch load. The implosion time for this MagLIF load is ~113 ns. There is minimal current loss in the MITL or convolute because of the low rate-of-change of inductance (dL/dt) of the MagLIF load.

Fig. 31 shows the energy balance for the MagLIF load. The energy balance in the vacuum section is shown with the energy reaching the insulator stack (blue curve), the energy past the MITL's (red curve), and the kinetic energy in the MagLIF liner (green curve). The total energy reaching the insulator stack

was 530 kJ. The energy past the MITL's was 375 kJ. The kinetic energy in the MagLIF load was ~100 kJ. The low level of kinetic energy in the load is a result of the small initial radius of the load and the small change in inductance seen during the implosion. The simulations gave a final implosion velocity of ~8 cm/µs using a convergence ratio of 6:1 [4,6].

The value of current when the liner reaches a minimum diameter of ~0.5 mm is ~11 MA for the 85-kV charge case. The surface magnetic field on the liner will be ~9 kT.

Extending these results to a full 100-kV charge voltage on the bricks would increase the peak current delivered to the load by 17.6% to 14.35 MA. This would make it possible for the radius of the MagLIF load to be increased to ~0.33 cm while holding the Be thickness constant and implosion time constant.

4. Pulsed-power performance analysis

This 15-TW LTD architecture, with an optimal 0.125-Ω driving impedance, is the most-efficient, imploding-load driver ever designed. This design stores 2 MJ of electrical energy in the capacitors at a ±85-kV charge. Of that 2 MJ of stored energy, ~1.7 MJ or 83.5% is calculated to reach the constant-impedance water transmission lines. A total energy of 1 MJ is
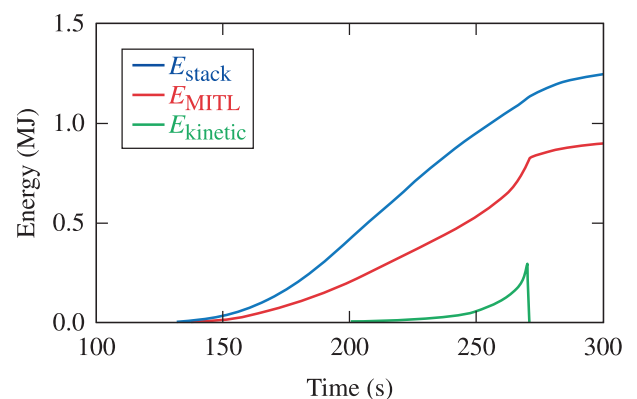

Fig. 31. Plot of the energy reaching the insulator stack (blue), the energy past the MITL's (red), and the kinetic energy of the magnetized liner inertial fusion (MagLIF) liner (green).
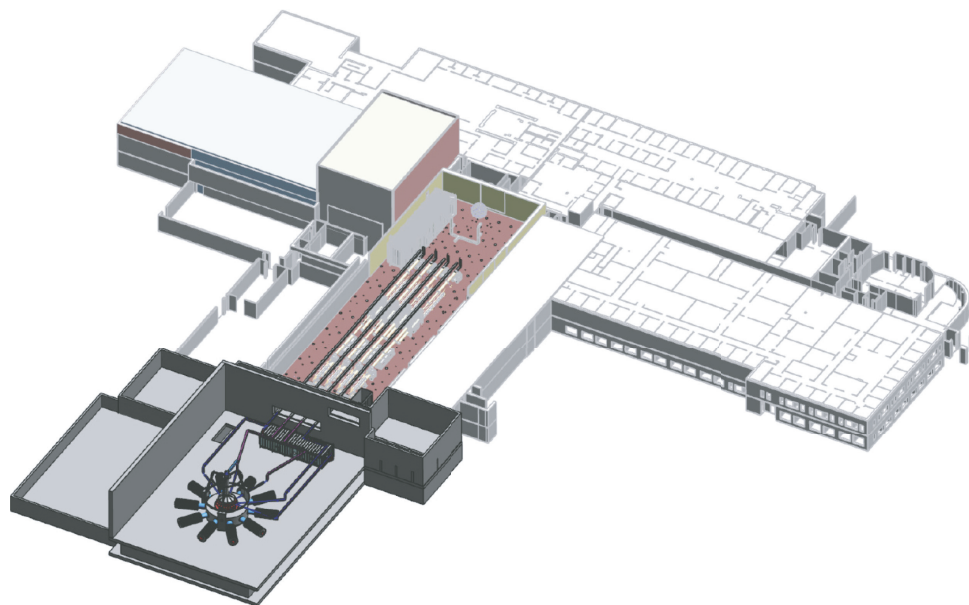
Fig. 32. Building overview highlighting beam paths to the chamber.

delivered past the insulator stack into the vacuum section of the accelerator for the case of a Z-pinch load with a total vacuum inductance of 10.82 nH. Approximately 450 kJ ends up as kinetic energy in the Z-pinch load out of the 1 MJ of energy available. This means that our design is 22.5% efficient in coupling stored electrical energy to the kinetic energy of the imploding load. This is the highest efficiency of any machine design to date. The radiation power out of the Z pinch is estimated to be ~60 TW or 4.5 × the peak electrical power.

The pulsed-power design works well for MagLIF loads even though the inductance of the load is higher than the Z-pinch load. There are no power-flow losses predicted in the MITL's. We expect that we could drive a range of MagLIF parameters without difficulty.

Short-circuit calculations show that this LTD design could easily drive the low-inductance short-circuit loads needed for equation-of-state (EOS) experiments [28]. These experiments require current pulse shaping (individual triggering of groups of bricks in each cavity). It remains to be seen how effective pulse shaping would be in an LTD architecture.

The utility and programmatic value of a 10- to 12-MA accelerator is greatly increased by the availability of a state-of-the-art laser diagnostic capability. In particular, such laser diagnostics would be invaluable for EOS experiments and vacuum power-flow measurements.

5. Description of laser capabilities

The system provides an opportunity to couple multiple state-of-the-art high-power laser beams to a pulsed-power machine (see Fig. 32). This unique configuration enables.

- multiple equatorial ultraviolet (UV) laser beams for 3-D radiography of an implosion driven by a 10-MA pulsed-power machine;

Table 1
Long-pulse beam requirements.

System parameter	Specification
Maximum UV on-target energy (10-ns square)	5000 J
Maximum UV on-target power (<10-ns pulses)	1.25 TW
Timing accuracy (rms)	<50-ps rms
Pointing accuracy (rms)	<150-μm rms
Focal-spot size	0.2 μm to 1 μm
Depth of focus	>5 mm
Beamline-limited shot rate	90 min
Pulse shaping	Arbitrary, 0.13−10 ns, ≤0.1-ns sampling
Pointing locations	TCC up to ~10 cm radically and up to ~10 cm vertically

Table 2
Short-pulse beam requirements.

System parameter	Tentative specification
Maximum intensity on target	5×10^{18} W/cm^2
Pulse-width range	1 to 100 ps
Maximum energy at best compression	400 J (or maximum power)[a]
Maximum energy at 10 ps	1250 J (or maximum power)[a]
Maximum energy at 100 ps	2600 J
Timing accuracy	<20 ps
Pointing accuracy	<150 μm [at off-axis parabola (OAP) focus]
Focal-spot size	R_{80} < 150 μm at OAP focus, with modification possible via either ellipsoidal refocusing or variable defocus
Beamline-limited shot rate	90 min
Temporal contrast	<10^{-11} (intensity)
Pointing locations	TCC up to ~10 cm radially

[a] *B*-integral−limited power will be determined by the final design for optic protection.

- a polar UV high-energy (5-kJ) laser with advanced beam conditioning for coupling to low-density plasmas (MagLIF);
- a single high-intensity, short-pulse beam for high-photon-energy (>10-keV) probing of dense materials; and
- novel debris-mitigation concepts to maintain laser performance and operations of multiple shots per day.

The laser will deliver four beams, each capable of independently providing a kilojoule-class beam to the pulsed-power load. All four beams are capable of nanosecond ("long-pulse") operation and will be frequency converted to 3ω. Two of the beams are additionally capable of operating with a broadband, optical parametric chirped-pulse-–amplification (OPCPA) front end that can be recompressed to picosecond pulses ("short pulse"). All four beams will be available in long-pulse, UV mode and an auxiliary grating compression chamber will be installed next to the pulsed-power chamber to operate one beam in short-pulse mode. The laser requirements are listed in Tables 1 and 2.

6. Summary

We have described the detailed conceptual design for an LTD accelerator capable of delivering an electrical power of 15 TW. The LTD portion of the design is based on prior LTD developments at Sandia National Laboratories [6]. The designs of the water transmission lines, the vacuum insulator stack, and the magnetically insulated transmission lines are all based on the successful Z and Z machines.

We have conducted extensive circuit simulations using *Screamer* models that have been validated by similar circuit simulations done for Z. These simulations suggest that the pulsed-power scaling laws for the water transmission lines, the insulator stack, and the MITL's used for the design are reasonable and are consistent with other successful pulsed-power designs. Circuit simulations predict a peak current of 10 MA into a 10.8-nH Z-pinch load and 12.5 MA into a 14.7-nH MagLIF load. The Z-pinch load reaches a kinetic energy of ~450 kJ and is expected to emit ~650 kJ of X rays in a 60-TW pulse.

Such a pulsed-power driver could be the first large-scale demonstration of LTD architecture and will be capable of high-quality science relevant to a number of DOE missions and serve as "prototype" of a future, more-capable pulsed-power facility. Coupling a 10-MA pulsed-power machine with modern lasers will provide a novel experimental/diagnostic platform. The platform will enable advanced X-ray sources at both low (<10-keV) and high (>10-keV) photon energies that will be used to study material opacities, dynamic diffraction, and Rayleigh–Taylor growth. Such a facility will also be capable of generating relevant currents that are of particular interest to pulsed-power machine physics including vacuum power flow and the development of "stand-off" concepts for future facilities that are designed for multi-megajoule fusion output. Such a facility in conjunction with smaller university based facilities could also play an important role in training students and developing and expanding the pulsed-power HEDP community.

This report was prepared as an account of work sponsored by an agency of the U.S. Government. Neither the U.S. Government nor any agency thereof, nor any of their employees, makes any warranty, express or implied, or assumes any legal liability or responsibility for the accuracy, completeness, or usefulness of any information, apparatus, product, or process disclosed, or represents that its use would not infringe privately owned rights. Reference herein to any specific commercial product, process, or service by trade name, trademark, manufacturer, or otherwise does not necessarily constitute or imply its endorsement, recommendation, or favoring by the U.S. Government or any agency thereof. The views and opinions of authors expressed herein do not necessarily state or reflect those of the U.S. Government or any agency thereof.

Appendix. *Screamer* run deck–Z-pinch implosion

```
PRE-CONCEPTUAL DESIGN OF THE 15-TW ACCELER-
ATOR – Rev 2
!
! Following Mazarakis, Spielman, Kim, and colleagues, the
design assumes LTD-module drivers
!
! The design presented below is a single-line model of the
machine
!
TIME-STEP 0.1E-9
RESOLUTION-TIME 0.1E-9
END-TIME 1.0E-6
NUMBER-PRINTS 5
EXECUTE-CYCLES ALL
ECHO YES
GRIDS NO
MAX-POINTS 5001
DETAIL-PRINTS FULL
!
BRANCH
```

```
!
!      *********      10      LTD      modules
*********************************************
!
! We begin with a model of 10 LTD modules, connected in
parallel
!
! We assume each LTD module consists of 16 LTD cavities,
connected in series
!
! We assume each cavity includes 22 LTD bricks, in parallel
!
! Each brick is assumed to have a 40-nF capacitance and a
160-nH inductance
! We assume a capacitor ESR of 0.13 Ω
! Ctot = 40nF × 22 × 10/16 = 0.55 μF
! Vtot = 85 kV × 2 × 16 = 2.72 MV
! Ltot = 160 nH × 16 / 22 × 10 = 11.64 nH
! Rtot = (0.13 Ω × 2 + 0.04) × 16/22 × 10 = 21.81 mΩ
!
! We use for this calculation the RLC-circuit model of an LTD
system that was
! developed by Mazarakis, Spielman, and colleagues
!
! We assume a single core loss resistance of 115 Ω per cavity
! Thus, the core loss for the entire machine is:
! Rloss = 115 × 13/10 = 184 Ω
!
! Note: the matched load per module is R = (1.7/
22) × 16 = 1.24 Ω
!
! We assume an LTD-system capacitance of 0.55 uF:
!
RCG 1.00E12 0.55E-6
!
! We assume each LTD cavity is charged to +/− 85 kV:
!
INITIAL VC1 2.72E6
!
! We assume the series resistance of the LTD system is
21.81 mΩ.
! and the series inductance is 11.64 nH:
!
RLS 21.81E-3 11.64E-9
!
! We assume the shunt resistance due to the cores is 149.5 Ω:
!
RCG 184 1.0E-12
!
! ******** 10 coaxial water-transmission-lines ********
!
! We assume that each of the 10 modules has a 54-ns coaxial
water TL
!
! We also assume that at this point, the impedance of a single
TL is 1.25 Ω. The impedance
! at the system output is 0.125 Ω
```

```
! We will need to add the TL losses in the water at some point
!
TRL LIN 54.0E-9 0.125
!
UFO VIN
$VTRIN
UFO IIN
$ITRIN
UFO PIN
$PTRIN
UFO EIN
$ETRIN
!
! ******** 10 coaxial to tri-plate water-transmission-lines
********
!
! We assume that each of the 10 modules has a 54-ns convo-
lution in the water TL
!
! We also assume that at this point, the impedance of a single
TL is 1.25 Ω. The impedance
! at the system output is 0.125 Ω
!
TRL LIN 54.0E-9 0.125
!
!      ***********************      Water      flares
****************************
!
TRL LIN 5.96E-9 0.125 0.240
!
UFO VOUT
$VWF
UFO IOUT
$IWF
UFO POUT
$PWF
UFO EOUT
$EWF
!
!
!
!      *********************      Insulator      stack
***************************
! The water/vacuum interface Router = 1.5 m, Rinner = 1.4
m, height = 11 cm (1 cm grading rings)
! Two stacks in parallel
!
RLS 1.0E-12 0.75E-9
!
UFO VOUT
$VSTACK
UFO IOUT
$ISTACK
UFO POUT
$PSTACK
UFO EOUT
$ESTACK
```

!
! ************************ Vacuum flares
****
!
RLS 1.0E-12 0.95E-9
!
UFO VOUT
$VVF
UFO IOUT
$IVF
UFO POUT
$PVF
UFO EOUT
$EVF
!
! *************************** MITLs
****
!
RLS 1.0E-12 4.67E-9
!
UFO VOUT
$VMITLS
UFO IOUT
$IMITLS
UFO POUT
$PMITLS
UFO EOUT
$EMITLS
!
! ***** Z-flow current loss immediately upstream of the
convolute ******
!
! We assume the MITL system has a Z-flow impedance of
1.20 Ω for two levels:
!
RCG 0.0001 1.00E-12
VARIABLE R1 POS-MODEL
! TSW CURSW TOPEN ZFLOW GSWMIN GSWMAX
CBFLAG
2E-9 1E2 2E-9 1.20 0.0001 10000 0
!
UFO IR1
$IZFLOSS
UFO R1
$RLOSS
!
! *************************** Convolute
****
!
RLS 0.0 0.650E-9
!
! ***************** Inner-MITL, coax, and pinch at
t = 0 *****************
! THE INNER MITL INDUCTANCE Disk from PHC
! Router = 7.1 cm, Rinner = 2.5 cm, gap = 0.4 cm
!
RLS 0.0 1.04E-9

RLS 0.0 1.98E-9
UFO IR2
$I_inner_mitl
RCG 1e12 0.0
UFO VR1
$V_inner_mitl
!
! The lower coax INDUCTANCE Router = 2.5 cm,
Rinner = 2 cm, height = 0.5 + 1.25 cm
! this is to the base of the load
!
RLS 0.0 0.781E-9
RCG 1e12 0.0
UFO VR1
$V_coax
!
! THE INITIAL PRS Load Inductance 2 cm height, 2 cm wire
array radius, 0.5 cm AK gap
!
RLS 0.0 0.89E-9
!
! ********* Time-dependent z-pinch model
****
!
! We choose a 2-cm initial radius, a 2-cm length, 1-mg mass,
and a 20:1 convergence ratio
!
! INITIAL R LENGTH TOTAL MASS FINAL R
CYLFOIL 0.02 0.02 1.5e-6 0.001
!
!
UFO FRAD
$RADIUS
!
UFO FVEL
$VELOCITY
!
UFO FKE
$EKINETIC
!
UFO VIN
$VLOAD
!
UFO IIN
$ILOAD
!
UFO EIN
$ELOAD
!
UFO PIN
$PLOAD
!
UFO L2
$LLOAD
!
UFO R2
$RLINER

```
!
UFO VR2
$VLINER
!
UFO PR2
$PLINER
!
!
!   ********   Tie   it   all   back   to   ground
*******************************
!
!
RCG 1.0E-12 1.0E-12!
```

References

[1] M.E. Savage, L.F. Bennett, D.E. Bliss, W.T. Clark, R.S. Coats, et al., An overview of pulse compression and power flow in the upgraded Z pulsed power driver, in: E. Schamiloglu, F. Peterkin (Eds.), 16th IEEE International Pulsed Power Conference, vol. 2, IEEE, New York, 2007, p. 979. http://ieeexplore.ieee.org/document/4652354/.

[2] M.E. Savage, K.R. LeChien, M.R. Lopez, B.S. Stoltzfus, W.A. Stygar, et al., Status of the Z pulsed power driver, in: 18th IEEE International Pulsed Power Conference, Omnipress, Piscataway, NJ, 2011, p. 983. http://ieeexplore.ieee.org/document/6191629/.

[3] D.B. Sinars, G.R. Bennett, D.F. Wenger, M.E. Cuneo, D.L. Hanson, et al., Monochromatic X-ray imaging experiments on the sandia national laboratories Z facility (invited), Rev. Sci. Instrum. 75 (2004) 3672. P.K. Rambo, I.C. Smith, J.L. Porter, M.J. Hurst, C.S. Speas, et al, Z-Beamlet: A multikilojoule, terawatt-cass laser system, Appl. Opt. 44 (2005) 2421, http://ao.osa.org/abstract.cfm?URI=ao-44-12-2421; G.R. Bennett, I.C. Smith, J.E. Shores, D.B. Sinars, G. Robertson, et al, 2–20 ns interframe time 2-frame 6.151 keV X-ray imaging on the recently upgraded Z Accelerator: A progress report, Rev. Sci. Instrum. 79 (2008) 10E914, http://scitation.aip.org/content/aip/journal/rsi/79/10/10.1063/1.2956823; B. W. Atherton, I.C. Smith, R.G. Adams, G.R. Bennett, D.V. Campbell, et al, Z-Beamlet: A multi-kJ, TW-class laser for backlit x-radiography applications on the Z-Accelerator, Sandia National Laboratories, Albuquerque, NM, Report SAND2007-5661C (2007), http://www.osti.gov/scitech/servlets/purl/1147451, http://scitation.aip.org/content/aip/journal/rsi/75/10/10.1063/1.1779607.

[4] S.A. Slutz, M.C. Herrmann, R.A. Vesey, A.B. Sefkow, D.B. Sinars, et al., Pulsed-power-driven cylindrical liner implosions of laser preheated fuel magnetized with an axial field, Phys. Plasmas 17 (2010) 056303. http://aip.scitation.org/doi/full/10.1063/1.3333505.

[5] M.G. Mazarakis, R.B. Spielman, A compact, high-voltage E-beam pulser, in: C. Stalling, H. Kirbie (Eds.), 12th IEEE International Pulsed Power Conference, vol. 1, IEEE, Piscataway, NJ, 1999, p. 412. http://ieeexplore.ieee.org/document/825498/. A.A. Kim, B.M. Koval'chuk, High power direct driver for Z-pinch loads, First International Congress on Radiation Physics, High Current Electronics, and Modification of Materials, Vol. 2, Springer, Berlin, 2000, p. 263; M.G. Mazarakis, R.B. Spielman, K.W. Struve, F.W. Long, A new linear inductive voltage adder driver for the saturn accelerator, Proceedings of the XX International Linac Conference, A.W. Chao, S.S.L. Yu, R.D. Ruth (Eds.), Stanford Linear Accelerator Center, Stanford, CA, 2000, p. 497, http://www.slac.stanford.edu/econf/C000821/TUC05.pdf; M.G. Mazarakis, R.B. Spielman, K.W. Struve, F.W. Long, Ultrafast LTD's for brems diodes and Z-pinch, 13th IEEE International Pulsed Power Conference, M.A. Newton, R.E. Reinovsky (Eds.), IEEE, Piscataway, NJ, 2001, p. 572, http://ieeexplore.ieee.org/stamp/stamp.jsp?arnumber=961407; M.G. Mazarakis, W.E. Fowler, K.L. LeChien, F.W. Long, M.K. Matzen, et al, High-current linear transformer driver development at Sandia

National Laboratories, IEEE Trans. Plasma Sci. 38 (2010) 704, http://ieeexplore.ieee.org/document/5373875/.

[6] W.A. Stygar, T.J. Awe, J.E. Bailey, N.L. Bennett, E.W. Breden, et al., Conceptual designs of two petawatt-class pulsed-power accelerators for high-energy-density-physics experiments, Phys. Rev. ST Accel. Beams 18 (2015), 110401, http://link.aps.org/doi/10.1103/PhysRevSTAB.18.110401.

[7] M.L. Kiefer, M.M. Widner, Screamer—a single-line pulsed-power design tool, in: P.J. Turchi, M.F. Rose (Eds.), Fifth IEEE Pulsed Power Conference, IEEE, Piscataway, NJ, 1985, p. 685. https://inis.iaea.org/search/search.aspx?orig_q=RN:18080265.

[8] R.B. Spielman, Y. Gryazin, Screamer v4.0—a powerful circuit analysis code, 2015, in: IEEE Pulsed Power Conference (PPC), IEEE, Piscataway, NJ, 2015. https://www.ieee.org/conferences_events/conferences/conferencedetails/index.html?Conf_ID=33290.

[9] R.B. Spielman, F. Long, T.H. Martin, J.W. Poukey, D.B. Seidel, et al., PBFA II-Z: a 20-MA driver for Z-pinch experiments, in: W.L. Baker, G. Cooperstein (Eds.), Tenth IEEE International Pulsed Power Conference, vol. 1, IEEE, New York, 1995, p. 396. http://ieeexplore.ieee.org/xpl/tocresult.jsp?filter%3DAND%28p_IS_Number%3A13049%29&refinements=4226002663&pageNumber=1&resultAction=REFINE.

[10] R.B. Spielman, S.F. Breeze, C. Deeney, M.R. Douglas, F. Long, et al., PBFA Z: a 20-MA Z-pinch driver for plasma radiation sources, in: K. Jungwirth, J. Ullschmied (Eds.), Proceedings of the 11th International Conference on High Power Particle Beams, vol. I, Institute of Plasma Physics, Czech Academy of Sciences, Prague, Czech Republic, 1996, p. 150. http://ieeexplore.ieee.org/stamp/stamp.jsp?arnumber=6308264.

[11] R.B. Spielman, C. Deeney, G.A. Chandler, M.R. Douglas, D.L. Fehl, et al., Z: a precision 200-TW, 2-MJ Z-pinch X-ray source, Bull, Am. Phys. Soc. 42 (1997) 1947. http://flux.aps.org/meetings/YR97/BAPSDPP97/abs/S4000002.html.

[12] R.B. Spielman, W.A. Stygar, K.W. Struve, J.F. Seamen, PBFA Z: a 55 TW/4.5 MJ electrical generator, in: M. Comyn, M.K. Craddock, M. Reiser, J.J. Thomson (Eds.), Proceedings of the 1997 Particle Accelerator Conference, vol. 1, IEEE, Piscataway, NJ, 1997, p. 1235. http://ieeexplore.ieee.org/xpl/mostRecentIssue.jsp?punumber=6051.

[13] M.E. Savage, M.G. Mazarakis, K.R. LeChien, B.S. Stoltzfus, W.A. Stygar, et al., Temporally shaped current pulses on a two-cavity linear transformer driver system, in: 18th IEEE International Pulsed Power Conference, Omnipress, Piscataway, NJ, 2011, p. 844. http://ieeexplore.ieee.org/document/6191525/.

[14] D.D. Bloomquist, R.W. Stinnett, D.H. McDaniel, J.R. Lee, A.W. Sharpe, et al., Saturn, a large area X-ray simulation accelerator, in: B.H. Bernstein, P.J. Turchi (Eds.), 6th IEEE Pulsed Power Conference, IEEE, New York, 1987, p. 310. R.B. Spielman, R.J. Dukart, D.L. Hanson, B.A. Hammel, W.W. Hsing, M.K. Matzen, J.L. Porter, Z-pinch experiments on Saturn at 30 TW, AIP Conf. Proc. 195 (1989) 3, http://aip.scitation.org/doi/abs/10.1063/1.38844.

[15] K. LeChien, M. Mazarakis, W. Fowler, W. Stygar, F. Long, et al., A 1-MV, 1-MA, 0.1-Hz linear transformer driver utilizing an internal water transmission line, in: 17th IEEE International Pulsed Power Conference, IEEE, Piscataway, NJ, 2009, p. 1186. http://ieeexplore.ieee.org/stamp/stamp.jsp?arnumber=5386430. M.G. Mazarakis, M.E. Savage, W.E. Fowler, L.F. Bennett, M. Jones, et al, Experimental validation of the first 1-MA water-insulated MYKONOS LTD voltage adder, in: 18th IEEE International Pulsed Power Conference, Piscataway, NJ, 2011, http://ieeexplore.ieee.org/document/6191552/.

[16] J.R. Woodworth, J.A. Alexander, F.R. Gruner, W.A. Stygar, M.J. Harden, et al., Low-inductance gas switches for linear transformer drivers, Phys. Rev. ST Accel. Beams 12 (2009) 060401. http://link.aps.org/doi/10.1103/PhysRevSTAB.12.060401.

[17] J.R. Woodworth, W.A. Stygar, L.F. Bennett, M.G. Mazarakis, H.D. Anderson, et al., New low inductance gas switches for linear transformer drivers, Phys. Rev. ST Accel. Beams 13 (2010) 080401. http://link.aps.org/doi/10.1103/PhysRevSTAB.13.080401.

[18] F. Gruner, W. Stygar, B. Stoltzfus, J. Woodworth, M. Abdalla, et al., PPPS-2013: a robust, low-inductance, low-jitter switch for petawatt-class pulsed power accelerators, in: Abstracts IEEE International Conference

on Plasma Science (ICOPS), IEEE, San Francisco, CA, 2013. http://ieeexplore.ieee.org/xpl/articleDetails.jsp?arnumber=6635032.

[19] A.A. Kim, M.G. Mazarakis, V.A. Sinebryukhov, B.M. Kovalchuk, V.A. Visir, et al., Development and tests of fast 1-MA linear transformer driver stages, Phys. Rev. ST Accel. Beams 12 (2009) 050402. http://stacks.iop.org/1367-2630/13/i=8/a=085005. A.A. Kim, M.G. Mazarakis, V.I. Manylov, V.A. Vizir, W.A. Stygar, Energy loss due to eddy current in linear transformer driver cores, Phys. Rev. ST Accel. Beams 13 (2010) 070401, https://journals.aps.org/prab/abstract/10.1103/PhysRevSTAB.13.070401#fulltext.

[20] W.A. Stygar, T.C. Wagoner, H.C. Ives, Z.R. Wallace, V. Anaya, et al., Water-dielectric-breakdown relation for the design of large-area multi-megavolt pulsed-power systems, Phys. Rev. ST Accel. Beams 9 (2006) 070401. http://link.aps.org/doi/10.1103/PhysRevSTAB.9.070401.

[21] W.A. Stygar, J.A. Lott, T.C. Wagoner, V. Anaya, H.C. Harjes, et al., Improved design of a high-voltage vacuum-insulator interface, Phys. Rev. ST Accel. Beams 8 (2005) 050401. http://link.aps.org/doi/10.1103/PhysRevSTAB.8.050401.

[22] W.A. Stygar, H.C. Ives, T.C. Wagoner, J.A. Lott, V. Anaya, et al., Flashover of a vacuum-insulator interface: a statistical model, Phys. Rev. Spec. Top. Accel. Beams 7 (2004) 070401. http://journals.aps.org/prab/abstract/10.1103/PhysRevSTAB.7.070401.

[23] M.E. Savage, B.S. Stoltzfus, K.N. Austin, P.A. Jones, W.A. Stygar, et al., Performance of a radial vacuum insulator stack, in: IEEE Pulsed Power Conference (PPC), IEEE, Piscataway, NJ, 2015. http://ieeexplore.ieee.org/xpl/articleDetails.jsp?reload=true&arnumber=7296785.

[24] M.R. Gomez, M.E. Cuneo, J.P. Davis, R.W. Lemke, R.D. McBride, et al., A systematic study of current flow and impedance behavior in the Z machine double post-hole convolute, in: 19th IEEE Pulsed Power Conference, IEEE, Piscataway, NJ, 2013. http://ieeexplore.ieee.org/document/6627397/.

[25] R.B. Spielman, C. Deeney, G.A. Chandler, M.R. Douglas, D.L. Fehl, et al., Tungsten wire-array Z-pinch experiments at 200 TW and 2 MJ, Phys. Plasmas 5 (1998) 2105, http://dx.doi.org/10.1063/1.872881.

[26] M.L. Wisher, Sandia National Laboratories, Private Communication, 2016.

[27] T.H. Martin, J.F. Seamen, D.O. Jobe, Energy losses in switches, in: K.R. Prestwich, W.L. Baker (Eds.), Ninth IEEE International Pulsed Power Conference vol. 1, IEEE, New York, 1993, p. 463. http://ieeexplore.ieee.org/stamp/stamp.jsp?tp=&arnumber=513375.

[28] C.A. Hall, J.R. Asay, M.D. Knudson, W.A. Stygar, R.B. Spielman, et al., Experimental configuration for isentropic compression of solids using pulsed magnetic loading, Rev. Sci. Instrum. 72 (2001) 3587. http://scitation.aip.org/content/aip/journal/rsi/72/9/10.1063/1.1394178.

[29] D.L. Peterson, R.L. Bowers, J.H. Brownell, C. Lund, W. Matuska, et al., Application of 2-D simulations to hollow Z-pinch implosions, AIP Conf. Proc. 409 (1997) 201. http://aip.scitation.org/doi/abs/10.1063/1.53929.